



Review

# Recent Advances and Challenges in the Seismo-Electromagnetic Study: A Brief Review

Hongyan Chen <sup>1</sup> , Peng Han <sup>1,2,\*</sup> and Katsumi Hattori <sup>3,4</sup>

<sup>1</sup> Department of Earth and Space Sciences, Southern University of Science and Technology, Shenzhen 518055, China

<sup>2</sup> Guangdong Provincial Key Laboratory of Geophysical High-Resolution Imaging Technology, Southern University of Science and Technology, Shenzhen 518055, China

<sup>3</sup> Graduate School of Science, Chiba University, Chiba 263-8522, Japan

<sup>4</sup> Center for Environmental Remote Sensing, Chiba University, Chiba 263-8522, Japan

\* Correspondence: hanp@sustech.edu.cn; Tel.: +86-755-8801-5515

**Abstract:** Due to their potential application in earthquake forecasting, seismo-electromagnetic phenomena were intensively studied for several decades all over the world. At present, measurements from ground to space have accumulated a large amount of observation data, proving an excellent opportunity for seismo-electromagnetic study. Using a variety of analytical methods to examine past earthquake events, many electromagnetic changes associated with earthquakes have been independently reported, supporting the existence of pre-earthquake anomalies. This study aimed to give a brief review of the seismo-electromagnetic studies preceding earthquakes and to discuss possible ways for the application of seismo-electromagnetic signals at the current stage. In general, seismo-electromagnetic signals can be classified into electric and magnetic changes in the lithosphere and perturbations in the atmosphere. We start with seismo-electromagnetic research in the lithosphere, and then we review the studies in the lower atmosphere and upper atmosphere, including some latest topics that aroused intense scholarly interest. The potential mechanisms of seismo-electromagnetic phenomena are also discussed. It was found that although a number of statistical tests show that electromagnetic anomalies may contain predictive information for major earthquakes, with probability gains of approximately 2–6, it is still difficult to make use of seismo-electromagnetic signals efficiently in practice. To address this, finally, we put forward some preliminary ideas about how to apply the seismo-electromagnetic information in earthquake forecasting.

**Keywords:** seismo-electromagnetic phenomena; precursors; earthquake forecast



**Citation:** Chen, H.; Han, P.; Hattori, K. Recent Advances and Challenges in the Seismo-Electromagnetic Study: A Brief Review. *Remote Sens.* **2022**, *14*, 5893. <https://doi.org/10.3390/rs14225893>

Academic Editor: Stephan Havemann

Received: 26 October 2022

Accepted: 18 November 2022

Published: 21 November 2022

**Publisher's Note:** MDPI stays neutral with regard to jurisdictional claims in published maps and institutional affiliations.



**Copyright:** © 2022 by the authors. Licensee MDPI, Basel, Switzerland. This article is an open access article distributed under the terms and conditions of the Creative Commons Attribution (CC BY) license (<https://creativecommons.org/licenses/by/4.0/>).

## 1. Introduction

Earthquake forecast is one of the most challenging scientific issues. The key to earthquake forecasting is to find the precursors that help predict impending earthquakes [1]. Science presented the great unsolved scientific mysteries of our time in the Special Issue marking the journal's 125th anniversary. Whether earthquake precursors that can help in prediction exist is one of them. To date, there have been many studies on earthquake forecasts, and most of them adopt a catalog-based probabilistic approach [2–5]. Although a certain amount of precursory information is available in earthquake catalogs [6], earthquake forecasting, especially short-term prediction, is still far from adequate [7,8]. Nevertheless, non-seismological approaches may provide additional useful information and broaden the knowledge for prediction [9,10]. The content of earthquake precursors includes many physical parameters such as mechanical deformation, gas emissions, groundwater level variations, ground temperature variations, fluctuations of the electromagnetic field, and so on. The detection of electromagnetic perturbations before fault ruptures was proposed as a useful way to monitor crustal activities and it has been proven to be a promising

phenomenon preceding earthquakes. To date, there have been many reports on electromagnetic field changes associated with earthquakes in a very wide frequency range from megahertz to quasi-DC [11–13]. These phenomena, known as seismo-electromagnetic phenomena, have been intensively studied for some decades [12,14–17] all over the world, from measurements on the ground to space detection. Based on the observation instruments in different spheres of the earth, seismo-electromagnetic phenomena can generally be classified into electric and magnetic changes in the lithosphere (measurement on the surface and/or underground), perturbations in the lower atmosphere (measurement above the surface and below the ionosphere), and the upper atmosphere (partially ionized or fully ionized regions).

## 2. Seismo-Electromagnetic Phenomena in the Lithosphere

The seismo-electromagnetic phenomena in the lithosphere are commonly recorded by passive ground-based observations of electric fields and/or magnetic fields [18]. Early seismo-electromagnetic studies measured perturbations of the electric potential difference between two electrodes buried in the ground. The case study of an M5.6 earthquake (depth = 17 km) was reported by Miyakoshi [19]. The observation carbon rod electrodes were set at an epicentral distance of 3 km. They found that potential differences changed clearly prior to the earthquake. This kind of signal was known as the seismic electric signal (SES). The most famous SES may be the one reported from Greece by Varotsos, Alexoupoulos, and Nicomos (VAN) [20–22]. They observed anomalous electric signals on both short (10–200 m) and long (1–3 km) dipoles with electric field amplitudes of up to 20  $\mu\text{V}/\text{m}$  and durations of a few minutes prior to several moderate–large earthquakes [21]. Varotsos et al. [22] issued some predictions of earthquakes since 1990 using the SES. These predictions soon drew lots of attention and aroused active debates (see details in Vol. 23 Issue 11, *Geophysical Research Letters*, 1996). In addition to seismic electric signals in Greece, there are some examples of SES observed in various earthquake-prone areas worldwide [23]. Recently, the natural time analysis of geoelectric field and seismicity changes were combined to study the precursory SES activity [24,25].

Magnetic field changes associated with earthquakes were also observed. One of the most promising candidates is the measurement of ultralow frequency (ULF) electromagnetic phenomena (less than 1 Hz), because of their deeper skin depths [12,14,15]. To date, now, a large number of ULF electromagnetic phenomena associated with earthquakes have been reported [10,11,26–41]. One of the most well-known ULF seismo-magnetic phenomena was the magnetic field changes related to the Ms7.1 Loma Prieta earthquake that happened on 18 October 1989, reported by Fraser-Smith et al. [40]. They found that the amplitude of ULF magnetic fields, especially at the frequency of 0.01 Hz, began to increase significantly about two weeks before the main shock. Due to the limitations of observation equipment, only the averaged amplitude of the magnetic field in the horizontal component was registered, which made it very difficult to analyze detailed waveforms for further study. Other case studies of the 1988 Spitak earthquake (M6.9) and the 1993 Guam earthquake (M 8.0) reported by the Russian group [41] and the Japanese group [42], respectively, also showed potential changes in the magnetic field before earthquakes. Hattori et al. [43] analyzed the geomagnetic data associated with the 1997 Kagoshima earthquakes (M6.5 and M6.3). By employing several reference stations, they eliminated the influence of global ionospheric disturbances and detected anomalous changes in the magnetic field, possibly related to the two large earthquakes.

The 2000 Izu earthquake swarm was another important case for seismo-electromagnetic study, as there were both electric and magnetic measurements in the vicinity of the epicenters. By analyzing these data simultaneously, Uyeda et al. [44] reported very robust results for seismo-electromagnetic phenomena. The ratio of electric potential between the two different observation dipoles at the frequency of 0.01 Hz has shown clear anomalous changes about two months before the earthquake swarm. These anomalies were unique against a 3-year-long background. The principal component analysis (PCA) of geomagnetic

data also showed anomalies before the swarm. The electromagnetic phenomena associated with the 2000 Izu earthquake swarm may be one of the most plausible results, as many reports have been published using different kinds of methodologies, such as PCA [44,45], singular spectral analysis (SSA) [46], fractal analysis [31,47,48], spectral density analysis [49], and direction-finding analysis [26]. In general, in addition to the above methods used for seismo-electromagnetic anomaly recognition, there are also other methods such as polarization analysis [49,50], wavelet analysis [51], diurnal variation analysis [35], and so on.

Whether these magnetic anomalies contain precursory information and how they can improve the forecasting of sizable earthquakes were not fully discussed. A sensitive geomagnetic network was installed in Kanto, Japan, to verify and clarify the ULF electromagnetic phenomena preceding large earthquakes. Plenty of data associated with moderate-large earthquakes have been accumulated. Researchers have analyzed the geomagnetic data observed during the past decade in the Izu and Boso Peninsulas. Hattori et al. [52] conducted some statistical studies of ULF seismo-magnetic phenomena in these areas and verified the correlation between ULF magnetic anomalies and sizeable local earthquakes. Previous studies showed that the earthquake-related magnetic signals may decrease with the epicentral distance and increase with the magnitude of the earthquake event [12,13,30,53], suggesting that augmenting earthquake forecasting with magnetic anomalies might involve their distance and magnitude dependences. The performance of trial forecasts based on ULF geomagnetic anomalies from the Kakioka Geomagnetic Observatory was evaluated by Han et al. [13]. They used the deep-night 0.01 Hz band data to avoid man-made noise, and the results showed that approximately 20% of the target earthquakes were preceded by the hypothesized type of magnetic anomaly related to the earthquake's occurrence. The authors rejected the concern that the successful forecasts were aftershocks and post-seismic disturbances of earthquakes, by demonstrating that trial forecasting based on recent seismicity is no better than random. Recently, Han et al. evaluated the optimal parameter for earthquake forecasting in the Kanto region, Japan [10], by utilizing long-term magnetic data observed in the region during the period 2000–2010 and applying Molchan's error diagram [54,55].

In the United States, a research project named QuakeFinder (QF) is carried out by the aerospace company Stellar Solutions. The goal was to develop a methodology to detect and analyze pre-earthquake electromagnetic (EM) signals in order to produce earthquake forecasts. As of April 2018, the array comprised 168 stations, most located in California, along the San Andreas Fault, and some located in Peru, Chile, Greece, and Sumatra [56]. The researchers discovered increases in ultra-low frequency magnetic pulse activity starting two weeks before the nearby seismic events in some cases and disappearing after the event [57]. The discovery is consistent with the statistical results of ULF seismo-magnetic phenomena in Japan [13]. In addition to the single earthquake's electromagnetic signals, some studies used 15+ years of data to statistically test whether electromagnetic signals do exist before significant earthquakes (close to the magnetometer stations) [58,59]. The algorithmic framework for investigating the temporal relationship of magnetic field pulses and earthquakes has been proposed, and some studies of searching for pre-earthquake signals such as long-term air ion monitoring have been investigated [58]. Recently, the case-control study on a decade of ground-based magnetometers in California conducted by QF and Google revealed signals in the frequency domain of 0.016–25 Hz before earthquakes [59], and the artificial intelligence method used can improve the efficiency and accuracy of anomaly detection. When compared to the statistical results of papers by Han et al. [13], the above results added to the evidence that there is a legitimate electromagnetic signal prior to medium-to-large earthquakes. However, more work needs to be conducted to refine the algorithms and to characterize and remove the known noise sources.

In China, a mobile geomagnetic monitoring network has been established in the last 20 years, covering most of the country's potential earthquake zones, and the geomagnetic anomaly provides very important support for the prediction of earthquake location [60]. Some research about the pre-seismic anomaly characteristics of geomagnetic changes was

reported. For example, the amplitude ratio of geomagnetic harmonic waves was significantly enhanced before the Ms5.5 Eryuan earthquake in 2013 [61], and the geomagnetic and geoelectric data show abnormal variations before the Wenchuan earthquake [33]. There were also some reports about the apparent resistivity changes before and after earthquakes [62–65]. The apparent resistivity change revealed by magnetotelluric (MT) measurements is a well-accepted technique, and some tests on the relation between earthquakes and apparent resistivity changes were revealed by repeated MT methods [66,67]. Further rigorous analysis based on continuous MT observation is required to ensure the reliability of the results.

On the other hand, some researchers claim that there were no electromagnetic changes prior to earthquakes. For example, Kappler et al. [68] analyzed the geomagnetic data associated with the 2004 Parkfield Earthquake (September 28, Mw 6.0, depth 8 km) by several methods, and they found no clear change of magnetic fields before the main shock. At present, there are still active debates in the geophysical community on seismo-electromagnetic phenomena [69–71].

### 3. Seismo-Electromagnetic Phenomena in the Lower Atmosphere

The seismo-electromagnetic phenomena in the lower atmosphere include atmospheric electric field perturbations, earthquake lights [72,73], thermal anomalies [74–76], and so on. The anomaly of atmospheric electric fields, possibly associated with earthquakes, is an interesting seismo-electromagnetic phenomenon in the lower atmosphere. There are some independent observations of earthquake-related anomalies of the atmospheric electric field after the Ms 7.8 Tangshan earthquake in China. To verify the reliability of the atmospheric electric precursors, one research group of the Institute of Geophysics has made continuous observations and carried out some studies on this topic since 1976. They obtained empirical relationships between the anomalies of the atmospheric electric field and earthquakes, and applied them to some earthquake prediction tests [77]. Recently, anomalous negative signals observed by ground-based atmospheric electric field instruments under fair weather conditions were considered a novel earthquake prediction approach [78]. One of the best-documented observations of earthquake lights is from Japanese earthquakes, where bright lights at the ground level were photographed from 20 to 200 m in diameter with a duration from 10 s to 2 min, restricted to mountain summits in a quartz-diorite faulted rock [73]. Luminous phenomena were reported, starting at approximately nine months before the 6 April 2009 earthquake and continuing until approximately five months after the shock [72]. A statistical study of lightning activity and  $M \geq 5.0$  earthquakes in the Taiwan region showed lightning activities tending to appear around the forthcoming epicenter and being enhanced a few days before shallow land earthquakes [79]. Possible explanations about earthquake lights include ultrashort-period air oscillations and generation of potential differences by the piezoelectric effect [80].

The thermal anomalies include atmospheric temperature, brightness temperature, surface latent heat flux (SLHF), outgoing longwave radiation, thermal infrared spectral range (TIR), etc. For example, the preseismic anomalies of SLHF were observed by Qin et al. [81], and they reported surface temperature anomalies before two major earthquakes [82]. Ouzounov et al. [76,83] reported thermal radiation anomalies associated with some major earthquakes, showing that infrared signals were observed near the epicenter areas and stayed from several hours to a few days. Genzano et al. [84] adopted the broadly used robust satellite technique data analysis methodology to identify the significant sequence of thermal anomalies acquired by multi-functional transport satellite (MTSAT) over Japan, confirming a noncausal correlation between anomalies and earthquakes. Tramutoli et al. [74] proposed a statistically well-founded definition of TIR anomalies for satellite TIR surveys. A probability gain of up to 3.7 was achieved as far as only significant sequences of TIR anomalies preceding earthquakes were considered. In practice, the remote sensing of thermal infrared anomalies can be affected by cloud coverage [85], and sometimes it is

hard to discriminate thermal contributions that are possibly connected to seismic activity in cloudy conditions [86].

#### 4. Seismo-Electromagnetic Phenomena in the Upper Atmosphere

The seismo-electromagnetic phenomena in the upper atmosphere are usually detected by using satellite observations and/or ground-based transmitter signals [17,87–91]. Since the 1990s, Hayakawa et al. continuously published some research papers that confirm the correlation between very low frequency (VLF) (3–30 kHz)/low frequency (LF) (30–300 kHz) radio signals and earthquakes [42,92–94]. They found significant shifts in the terminator times and phase before the main shock for the signal's propagation characteristics. Their statistical study suggested that the VLF/LF ionospheric perturbation in terms of amplitude (trend) show a statistically significant precursory behavior (3–5 days before the earthquake), and the enhancement of dispersion (fluctuation) is clearly visible for  $M \geq 6.0$  earthquakes. The statistical results also confirm and support previous results by Rozhnoi et al. [95]. The VLF from the direction of the source of earthquakes was reported by Asada et al. [96], though without establishing statistical significance as 'earthquake-preceding phenomena'. Five megahertz-sampling rates of VLF recorders were developed in Japan, and Nagao et al. determined the source location using the arrival time difference [97]. They examined the data for 5 days before and 1 day after an earthquake on 25 June 2017, and found seven similar pulses located within 20 km of the hypocenter. There was no light in that time window. There are also two sites observing VLF pulses, ultra-low frequency, and atmospheric electric fields at Kuroshio-town in Kochi, Japan [98]. In the past ten years, the application of ground-based and satellite signals in seismic monitoring was developed in China, and VLF/LF artificial source signal monitoring has become one of the main technical means of seismic disturbance analysis [99,100].

The French satellite DEMETER was the first seismo-electromagnetic satellite devoted to investigating seismo-electromagnetic phenomena. The pre-earthquake disturbances in the ionosphere were observed by the DEMETER satellite. Parrot et al. [101] and Sarkar et al. [17] demonstrated several examples of variations in the plasma parameters recorded by DEMETER satellites over the epicenters of earthquakes before their occurrence. Zeng et al. [102] analyzed the DEMETER data and their results indicated that the electron concentration, temperature, and oxygen ion changed rapidly 5 days before the Wenchuan earthquake. Akhoondzadeh et al. [103] investigated the electron and ion density variations before strong earthquakes ( $M > 6.0$ ) using DEMETER and GPS data. They found that the anomalous deviations prior to earthquakes had different signs from case to case, and their amplitude depended on the magnitude of the earthquake. There were positive and negative anomalies in both DEMETER and GPS-TEC data for 1–5 days before all the studied earthquakes during quiet geomagnetic conditions. These results were verified by subsequent studies [104–109], suggesting that the ionosphere might have some response prior to large earthquakes. Additionally, the VLF field intensity observed by the DEMETER satellite was found to be statistically significant [110]. The field intensity was found to take a minimum at the time when the satellite was closest to the epicenter of the upcoming earthquake. The pre-seismic changes were observed by satellite only after stacking many cases due to the noises.

After the DEMETER satellite ended in 2010, the European Space Agency launched the Swarm satellite in 2013. Marchetti et al. [111–113] reported the seismo-ionospheric anomalies from Swarm satellite data around the time of the strong earthquake and the worldwide statistical correlation of eight years of satellite data with  $M5.5+$  earthquakes. The precursory worldwide signatures study found some clear concentrations of electron density and magnetic anomalies from more than two months to some days before the earthquake occurrences, and the epicenter location was related to the detected anomalies [112,114]. There were also some reports about the detection of ionospheric signals in the region magnetically conjugate to the earthquake zone [115].

The China Seismo-Electromagnetic Satellite (CSES) mission, launched in 2018, is the first satellite in China to measure seismo-associated phenomena in the near-Earth electro-

magnetic environment, having a lot of application prospects in the study of seismology, geophysics, space sciences, and so on [91]. This was planned to operate for 5 years. During its five-year operation time, CSES records many kinds of data, such as multi-band waveform and the spectra of electric and magnetic fields; in situ plasma parameters (including the densities and temperatures of electrons and ions); electron density profiles and tomography; energetic particle flux and energy spectra. Many reports showed that the performance of the payload can satisfy the requirement of the scientific objectives of the mission [116–122]. Next, we discuss some of the last published results. Yan et al. [123] reported the observations of unusual ionospheric irregularities by CSES before four earthquakes. Zhang et al. [65] investigated ionospheric perturbations in very low-frequency transmitters recorded by CSES, and they claimed that the perturbations to the satellite were more likely related to the overlapped electric field in the earthquake preparation area. An investigation into the characteristics of pre-earthquake ionospheric effects related to four shallow-focus earthquakes in Indonesia was conducted by Song et al. [124]. Significant positive perturbations 1–7 days before earthquakes were revealed. Recently, Zhu et al. [125] published the CSES data analysis of electron density (Ne) and temperature (Te), to support a temporal-spatial correlation between the earthquakes and the observation of positive Ne variations/negative Te variations before the seismic events. Xiong et al. [126,127] and Zhong et al. [128] analyzed the pre-earthquake electromagnetic, ionospheric, or space electric field perturbations by machine learning. However, similarly to other reports on earthquake precursors, the anomalous variation of parameters has not been revealed in all studied earthquakes, and the perturbations seem to occur at various temporal and spatial distances to the earthquake. Other possible sources of the observed anomalies in the ionospheric and geomagnetic dynamics driven by solar activity may not be fully ruled out. On the other hand, the satellite orbits the earth at a high speed, and the observed anomalous variations cover a large zone even up to a 2000 km range. Overall, due to the relatively low resolution power, the applications based on the satellite may face a challenge of the better constraint size and location of earthquake preparation areas. Even though the reported analyses from CSES are not conclusive now, the second mission of the CSES series, CSES-02, will be launched in 2023. It will have the same multi-instrumental payload and similar orbital parameters as the first satellite, but will allow for reducing the revisit time of the same geographic region. The large number of observations will help in studying the frequencies, amplitudes, and characteristics of ionospheric perturbations related to earthquakes and generation mechanisms.

Among the seismo-electromagnetic phenomena in the ionosphere, anomalous changes in the ionospheric total electron content (TEC) are one of the most frequently reported phenomena preceding large earthquakes [129–140]. TEC is a measure of integrated density along a straight line between the satellite and ground GPS stations. One TEC unit (TECU) is equal to  $10^{16}$  electrons/m<sup>2</sup>. Various GPS stations can be utilized for ground-based TEC observations, including the International GNSS Station (IGS), the Crustal Movement Observation Network of China (CMONC), the GPS Earth Observation Network (GEONET), and so on. Two-dimensional TEC maps derived from ground-based observations are widely used, such as the data from the Center for Orbit Determination of Europe (CODE), and they are regarded as one of the most precise available Global Ionosphere Maps (GIM) and treated as a high-accuracy reference [141]. In contrast, space-borne TEC data are rare due to the lack of processing TEC data in the satellite platform. However, satellite systems can overcome the problem that ground stations are not available in the ocean [142], and act as a supplement to GIM-TEC.

The method to detect anomalies in the ionosphere includes the mean/median statistical envelope method [143,144], cubic fit analysis [140], pattern recognition analyses [139,145,146], etc. The mean/median statistical envelope methods use the N-day mean or median techniques to detect anomalies, becoming a common and popular method. However, there is no clear justification for the selection of N-day used in studies, and the method faces the challenge of accounting for TEC changes owing to different sources such

as space weather and seismic effects. The confidence level, which defines the normal ionospheric variations, also needs to be ascertained in the mean statistical envelope methods. The cubic fit analysis was adopted by Heki to obtain the anomalies about five TECU several hours/minutes before the 2011 Tohoku earthquake. The study indicated that similar pre-seismic TEC anomalies were seen in the 2010 Chile earthquake (Mw8.8), the 2004 Sumatra (Mw9.2), and the 1994 Hokkaido (Mw8.3) earthquake, but not in smaller earthquakes [140]. The anomalies even increased to 10 TECU before the Sumatra earthquake (Mw9.2). Some scholars point out that it might yield erroneous interpretations about anomalies [147,148]. Iwata and Umeno introduced the correlation analysis method and detected the pre-seismic TEC anomalies before the 2011 Tohoku earthquake and the 2016 Kumamoto earthquake, whose characteristic patterns do not depend on the choice of extrapolation functions for nonlinear regression [149,150].

In the research on seismo-electromagnetic phenomena in the ionosphere, the effects of other sources should be considered because the TEC perturbations are the integrated product of space weather and other kinds of sources such as earthquakes, tsunamis, volcanic eruptions [151], etc. The choice of space weather indices could be justified based on the location, depending on the data availability and station coverage [152]. When defining the space effect levels, some consensus values should be used based on the authoritative parameters from space physics, and all relevant space weather indices should be verified for quiet or low activity in order to ensure the space-related influences on ionospheric perturbations [142]. Some technological methods were developed to eliminate the effect of space weather activity without the use of arbitrary space indices to detect pre-earthquake TEC anomalies, including wavelet analyses [153], singular spectrum analysis [151,154], etc. In addition, demonstrating the three-dimensional structure of ionospheric disturbances can better reshape the morphological characteristics [155,156]. In general, it is very important to establish a reliable normal background field, exclude the interference effects, and identify reliable anomalies related to seismic activity [157].

In the review report of Pulinets et al. [16], the total electron content (TEC) over the epicenter usually increased or decreased for approximately 4–6 h on 1–5 days before earthquakes, and the TEC anomalous amplitude was related to the earthquake magnitude and local time, ranging from  $\pm 30\%$  to  $\pm 100\%$ . Meanwhile, some statistical investigations into the relationship between earthquakes and TEC anomalies were performed. Liu et al. [158] statistically examined the ionospheric plasma frequency (or electron density) in ionograms recorded by a local ionosonde and found that the critical frequency of the F2-peak, foF2, significantly decreased 1–5 days prior to 13  $M \geq 6.0$  earthquakes in Taiwan during the period 1994–1999. Kon et al. [159] analyzed the TEC anomalies before the earthquakes in Japan and found that the positive TEC anomalies were usually observed 1–5 days before  $Mw > 6.0$  earthquakes with a focal depth of less than 40 km. Hirooka et al. [135,136] found that the electron density in the F-layer decreased by approximately 6 TECU for 3 days before the earthquakes in the low geomagnetic latitudinal regions. Chen et al. [160] gave the statistical evidence that the electron density decreased 1–5 days before  $M \geq 6.0$  earthquakes in mainland China. Zhu et al. [161] found that the occurrence rates of TEC disturbances within 5 days before the inland earthquakes were higher than those after earthquakes, and the biggest difference of spatial distribution lies in the epicenter area. He and Heki [162] found possible ionospheric electron density enhancement detected before the large earthquakes by analyzing the vertical total electron content data observed by GNSS stations near epicenters, and these pre-seismic signals were mostly within 5 TECU. It is quite interesting to find that the TEC anomalies prior to large earthquakes can be either positive (Japan region) or negative (Taiwan region). In addition, TEC variability in seismically active regions is greater than in non-seismically active regions [142].

There are also some studies that focused on the changes associated with earthquakes in the magnetosphere, for example, a study of charged particle precipitation from van Allen radiation belts during a land earthquake and an ocean earthquake was reported [163]. Particle bursts (PBs) were found to be accumulated only around the earthquake day,

reaching their maximum on the day of the earthquake and with a complete absence of such events on days away from the event day. Some statistical studies showed significant bursts of high-energy particles observed by SOHO satellite in the magnetosphere before earthquakes [164]. In general, since the magnetosphere is mostly affected by solar activity, it might be more complicated to study seismo-electromagnetic phenomena there.

Regarding the preparation zone of the earthquake, the most widely used equation is  $R = 10^{0.43M_w}$ , where  $R$  is the radius (km) and  $M_w$  is the magnitude [165]. The equation gained only used 24 earthquake events and did not account for ionospheric anomalies, although the authors concluded that it could be used to estimate the effective precursor manifestation zone [165]. Based on data from Benioff (i.e., crustal) strains, Bowman et al. found that the exponent in the equation should be increased for  $M_w \geq 6.0$  earthquakes as they rupture the entire crust [166], so using the equation straightforwardly might result in errors. In addition, most scholars agreed that pre-earthquake TEC anomalies are most significant close to the epicenter [167], while other studies reported that they are greatest at the edge of the preparation zone [168]. Liu and Xu [169] revealed that the most perturbed ionospheric regions were located south of the epicenter and the zone was greater than 1000 km. Consequently, arguments have been put forward that earthquake preparation on the ionosphere/magnetosphere could have a larger radius [170]. The most complicated part of earthquake forewarning to use the ionosphere/magnetosphere perturbation is the large preparation zone based on the anomalies [142], so the surface observation should be combined to constrain potential earthquake locations.

## 5. Possible Mechanisms of Seismo-Electromagnetic Phenomena

To understand the mechanisms of seismo-electromagnetic phenomena in the lithosphere, various experiments and simulations have been conducted [171–181]. The mechanisms proposed for the generation of electromagnetic signals include: electrokinetic effects [182,183], piezo-electric effects [184], piezomagnetic effects [185], triboelectric effects [186], induction effects [187,188], microfracture effects [89,189], and P-holes [190–193]. For most of these models, electromagnetic signals are more or less related to stress or strain changes. The numerical simulation of coupled seismic and electromagnetic waves in multilayered porous media were developed to explain the coseismic electromagnetic signals [194,195]. However, field observations can hardly record strong, clear co-rupture signals [11]. The selectivity phenomenon of SES might explain why some electromagnetic anomalies are observed before earthquakes and others are not [175]. One of the most studied issues in the physics of earthquake precursors is the role of seismic-induced radon exhalation in the generation of electromagnetic disturbances. It has been proposed that the enhancement of the total rock surface due to failure would increase the emissions of radon and other gases from grains and facilitate migration. This would be in agreement with the enhancement of radon concentration observed in aftershocks and some laboratory experiments [196] which showed the growth of radon emissions of granites under compressional stress.

Although a number of studies have discussed possible mechanisms of pre-earthquake disturbances in the atmosphere [129,192], the generation process is still not well understood. Most hypotheses were based on the propagation of EM waves, which originated from the ground due to certain mechanisms such as piezo-electric effects [80], the triboelectric effect [186], and positive holes (P-holes) [190]. Pulinets and Boyarchuk [129] discussed a model based on the emissions of radioactive gases or metallic ions. Pulinets and Ouzounov [197] proposed a unified concept for the pre-earthquake atmospheric disturbances, named the “Lithosphere–Atmosphere–Ionosphere Coupling (LAIC)” model. According to the LAIC model, radon can generate local ionization in the lower layers of the atmosphere that can facilitate water vapor condensation, leading to the release of latent heat exhalation (that could explain thermal fluctuations) and local variation of the conductivity, thereby impacting the electric circuit over the earthquake preparation zone and generating the observed seismo-associated ionospheric anomalies. Harrison et al. [198] argued that enhanced ionization in the lower atmosphere would increase the vertical cur-

rent flow in fair weather, which might help understand earthquake–cloud coupling [199] through the global atmospheric electric circuit [200]. Kuo et al. [201,202] performed some numerical simulations and showed ionosphere plasma bubbles and density variations induced by pre-earthquake rock currents and associated surface charges. Other mechanisms including the atmospheric gravity waves (AGWs) triggered by gas releases or thermal anomalies [203] and electric current of seismic origin due to the convective transfer of charged soil aerosols [204,205] can also explain pre-earthquake disturbances in the atmosphere to some extent [206]. The coseismic lower atmospheric and ionospheric perturbation triggered by seismic waves through acoustic and/or gravity waves was verified for the M9.0 Tohoku earthquake [207].

Some researchers present a potential physics-based research approach that takes into account the interaction among observation, data processing methodology, and physical model [208]. The coupling between the lithosphere and atmosphere requires multiple instruments installed on and near the Earth’s surface and space satellites. Recently, a novel system for monitoring vibrations and perturbations in the lithosphere, lower atmosphere, and upper atmosphere was established in the countryside of Leshan City, Sichuan Province, China, in 2021 [209]. The system combines all kinds of observation instruments collecting data from the lithosphere and atmosphere, to gain abundant measurements across different layers preceding earthquakes. As a novel systematic observing platform, it can provide researchers with more information about the preparation process for forthcoming earthquakes in the future.

## 6. Applications of Seismo-Electromagnetic Signals in Earthquake Forecasting

There are some methods to evaluate whether the seismo-electromagnetic phenomena contain precursory information, among which the receiver operating characteristic (ROC) curve and Molchan’s error diagram are the two most widely used [160,210]. Statistical tests have shown that the electromagnetic anomalies may contain predictive information for major earthquakes, with probability gains of approximately 2–6 [74,160,210]. In addition to seismo-electromagnetic phenomena, other precursors were also observed. A representative event of which various geophysical precursors were documented is the 2011 Tohoku earthquake (Mw 9.0) [38,140,211–220]. Locations of seismo-geomagnetic anomalies in spatial distribution showed a good correlation with the epicenter of the earthquake [38,220]. These spatiotemporal results were consistent with those obtained from other independent observations such as the groundwater level and GPS displacements [219]. The related precursory characteristics of the earthquake are listed in the Table 1 below. The coupling of multiple pre-earthquake phenomena provides new insights on earthquake preparation process, suggesting that incorporating multi-geophysical information might be a possible means of improving earthquake forecast.

**Table 1.** Representative precursory characteristics before the 2011 Tohoku earthquake.

Observation	Leading Time	Characteristic	Reference
Seismic activity	23 years	Seismic quiescence in rupture region	(Katsumata, 2011 [211])
	6 years	Decade-scale decrease in b value	(Nanjo et al., 2012 [212])
	A few months	Seismicity exhibited distinct minima	(Sarlis et al., 2013 [213])
	1 month	Foreshock sequence and slow slip	(Kato et al., 2012 [214])
Deformation	2 months	Crustal movement changes	(Chen et al., 2014 [215])
	1 month	Slow slip event	(Ito et al., 2013 [216])
	1 month	GPS surface motion	(Hattori et al., 2014 [217])
Fluid	3 months	Groundwater level decrease	(Orihara et al., 2016 [218])
Geomagnetism	2 months	Geomagnetic diurnal variation changes	(Han et al., 2016 [219])
Ionosphere	40 min	TEC enhancement	(Heki, 2011 [140])

As the earthquake process is rather complex, the earthquake preparation phase cannot be easily monitored using a single approach. To improve the reliability of earthquake forecasting, the two following models that could integrate precursory information from different approaches were proposed. One is the earthquake model that combines self-exciting and mutually exciting elements from the Hawkes process [62,221,222]. The core idea of this combined model is that the status of the earthquake event at present is controlled by the event itself (self-exciting) and all the external factors (mutually exciting) in the past. The conditional intensity function is a time-varying point process with rate  $\lambda(t)$  written as

$$\lambda(t) = \mu + \lambda_s(t) + \lambda_E(t) \quad (1)$$

where  $\mu$  represents the constant background rate,  $\lambda_s(t)$  is the self-exciting term that models the information from past seismic events, and  $\lambda_E(t)$  is the external excitation term that models the information from non-seismic observations such as the seismo-electromagnetic anomalies. The other is a network model based on machine learning, where multi-geophysical precursor information is taken as the input layer, and the factors of earthquakes such as time, location, and magnitude are taken as the output layers, as shown in Figure 1. Some important features in discriminating pre-earthquake perturbations may be established by the machine learning network. Overall, the forecast model combining the integrated observations (shown in Figure 2) is a worthwhile study in the future.

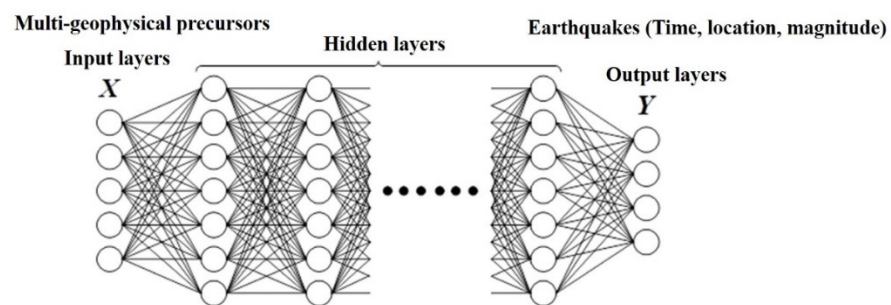


**Figure 1.** Earthquake forecast network based on machine learning.

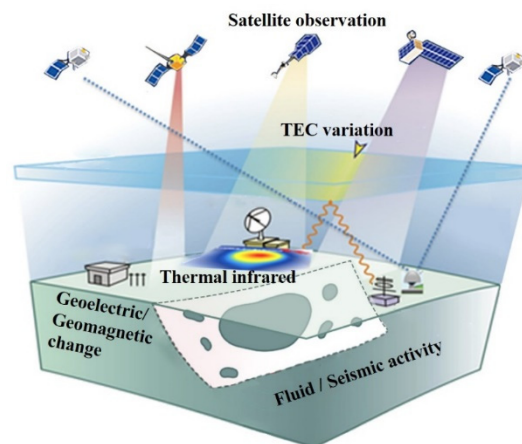


**Figure 2.** Multi-geophysical observation system for earthquake modeling and forecasting (modified from [83]).

## 7. Conclusions

As a kind of potential precursor of the earthquake, the seismo-electromagnetic phenomena were paid considerable attention and play a crucial role in the study of seismic hazards, although there are some controversial problems deserving further study. After reviewing the seismo-electromagnetic study in the lithosphere, the lower and upper atmosphere, and discussing the possible mechanisms, we present the related achievements

and the potential applications in implementing seismo-electromagnetic phenomena for earthquake forecasting. The challenges include the variability of the detected intensity, frequencies, spatial, and temporal distribution around the epicenter, etc. Since the electromagnetic signal contains certain pieces of precursor information, achieving a better understanding of the physics of seismo-electromagnetic phenomena and developing multi-geophysical integrated forecast models is worth the efforts being made by the scientific community worldwide.

**Author Contributions:** Conceptualization, P.H., K.H. and H.C.; methodology, H.C.; software, H.C.; validation, P.H. and K.H.; formal analysis, H.C.; investigation, H.C.; resources, P.H.; data curation, P.H.; writing—original draft preparation, P.H. and H.C.; writing—review and editing, P.H. and K.H.; visualization, H.C.; supervision, P.H. and K.H.; project administration, P.H.; funding acquisition, P.H. All authors have read and agreed to the published version of the manuscript.

**Funding:** This research is partly supported by National Natural Science Foundation of China (41974083), China Seismic Experimental Site (DQJB22Z01-09), Shenzhen Science and Technology Program (Grant No. KQTD20170810111725321), and Guangdong Provincial Key Laboratory of Geophysical High-Resolution Imaging Technology (2022B1212010002).

**Institutional Review Board Statement:** Not applicable.

**Informed Consent Statement:** Not applicable.

**Data Availability Statement:** Not applicable.

**Acknowledgments:** The authors would like to thank Jiancang Zhuang for helpful discussions.

**Conflicts of Interest:** The authors declare no conflict of interest.

## References

1. Ma, J. Whether earthquake precursors help for prediction do exist. *Sci. China Press Chin. Ed.* **2016**, *61*, 409–414.
2. Jordan, T.H. Earthquake predictability, brick by brick. *Seismol. Res. Lett.* **2006**, *77*, 3–6. [[CrossRef](#)]
3. Davis, C.; Keilis-Borok, V.; Kossobokov, V.; Soloviev, A. Advance prediction of the 11 March 2011 Great East Japan Earthquake: A missed opportunity for disaster preparedness. *Int. J. Disaster Risk Reduct.* **2012**, *1*, 17–32. [[CrossRef](#)]
4. Iacchetti, S.; Cremen, G.; Galasso, C. Validation of the epidemic-type aftershock sequence (ETAS) models for simulation-based seismic hazard assessments. *Seismol. Res. Lett.* **2022**, *93*, 1601–1618. [[CrossRef](#)]
5. Ogata, Y. Prediction and validation of short-to-long-term earthquake probabilities in inland Japan using the hierarchical space-time ETAS and space-time Poisson process models. *Earth Planets Space* **2022**, *74*, 110. [[CrossRef](#)]
6. Zhuang, J. Next-day earthquake forecasts for the Japan region generated by the ETAS model. *Earth Planets Space* **2011**, *63*, 207–216. [[CrossRef](#)]
7. Zechar, J.D.; Jordan, T.H. Testing alarm-based earthquake predictions. *Geophys. J. Int.* **2008**, *172*, 715–724. [[CrossRef](#)]
8. Shebalin, P.; Narteau, C.; Holschneider, M. From alarm-based to rate-based earthquake forecast models. *Bull. Seismolog. Soc. Am.* **2012**, *102*, 64–72. [[CrossRef](#)]
9. Wang, T.; Zhuang, J.; Kato, T.; Bebbington, M. Assessing the potential improvement in short-term earthquake forecasts from incorporation of GPS data. *Geophys. Res. Lett.* **2013**, *40*, 2631–2635. [[CrossRef](#)]
10. Han, P.; Zhuang, J.; Hattori, K.; Chen, C.-H.; Febriani, F.; Chen, H.; Yoshino, C.; Yoshida, S. Assessing the potential earthquake precursory information in ULF magnetic data recorded in Kanto, Japan during 2000–2010: Distance and magnitude dependences. *Entropy* **2020**, *22*, 859. [[CrossRef](#)]
11. Uyeda, S.; Nagao, T.; Kamogawa, M. Short-term earthquake prediction: Current status of seismo-electromagnetics. *Tectonophysics* **2009**, *470*, 205–213. [[CrossRef](#)]
12. Hattori, K. ULF geomagnetic changes associated with large earthquakes. *Terr. Atmos. Ocean. Sci.* **2004**, *15*, 329–360. [[CrossRef](#)]
13. Han, P.; Hattori, K.; Hirokawa, M.; Zhuang, J.; Chen, C.; Febriani, F.; Yamaguchi, H.; Yoshino, C.; Liu, J.; Yoshida, S. Statistical analysis of ULF seismomagnetic phenomena at Kakioka, Japan, during 2001–2010. *J. Geophys. Res.* **2014**, *119*, 4998–5011. [[CrossRef](#)]
14. Park, S.K. Precursors to earthquakes: Seismo-electromagnetic signals. *Surv. Geophys.* **1996**, *17*, 493–516. [[CrossRef](#)]
15. Johnston, M.J.S. Review of electric and magnetic fields accompanying seismic and volcanic activity. *Surv. Geophys.* **1997**, *18*, 441–476. [[CrossRef](#)]
16. Pulnits, S.A.; Legen'ka, A.D.; Gaivoronskaya, T.V.; Depuev, V.K. Main phenomenological features of ionospheric precursors of strong earthquakes. *J. Atmos. Sol. Terr. Phys.* **2003**, *65*, 1337–1347. [[CrossRef](#)]
17. Sarkar, S.; Gwal, A.K.; Parrot, M. Ionospheric variations observed by the DEMETER satellite in the mid-latitude region during strong earthquakes. *J. Atmos. Sol. Terr. Phys.* **2007**, *69*, 1524–1540. [[CrossRef](#)]

18. Hayakawa, M.; Molchanov, O.A.; Team, N.; Team, U.E.C. Summary report of NASDA's earthquake remote sensing frontier project. *Phys. Chem. Earth* **2004**, *29*, 617–625. [[CrossRef](#)]
19. Miyakoshi, J. Anomalous time-variation of the self-potential in the fractured zone of an active fault preceding the earthquake occurrence. *J. Geomagn. Geoelectr.* **1986**, *38*, 1015–1030. [[CrossRef](#)]
20. Varotsos, P.; Alexopoulos, K.; Nomicos, K.; Lazaridou, M. Earthquake prediction and electric signals. *Nature* **1986**, *322*, 120. [[CrossRef](#)]
21. Varotsos, P.; Alexopoulos, K.; Lazaridou, M. Latest aspects of earthquake prediction in Greece based on seismic electric signals, II. *Tectonophysics* **1993**, *224*, 1–37. [[CrossRef](#)]
22. Varotsos, P.; Alexopoulos, K.; Lazaridouvarotsou, M.; Nagao, T. Earthquake predictions issued in Greece by seismic electric signals since 6 February 1990. *Tectonophysics* **1993**, *224*, 269–288. [[CrossRef](#)]
23. Sarlis, N.V.; Varotsos, P.A.; Skordas, E.S.; Uyeda, S.; Zlotnicki, J.; Nagao, T.; Rybin, A.; Lazaridou-Varotsos, M.S.; Papadopoulou, K.A. Seismic electric signals in seismic prone areas. *Earthq. Sci.* **2018**, *31*, 44–51. [[CrossRef](#)]
24. Sarlis, N.V.; Skordas, E.S. Study in natural time of geoelectric field and seismicity changes preceding the Mw6.8 earthquake on 25 October 2018 in Greece. *Entropy* **2018**, *20*, 882. [[CrossRef](#)] [[PubMed](#)]
25. Sarlis, N.V.; Skordas, E.S.; Christopoulos, S.-R.G.; Varotsos, P.A. Natural time analysis: The area under the receiver operating characteristic curve of the order parameter fluctuations minima preceding major earthquakes. *Entropy* **2020**, *22*, 583. [[CrossRef](#)] [[PubMed](#)]
26. Ismaguilov, V.S.; Kopytenko, Y.A.; Hattori, K.; Hayakawa, M. Variations of phase velocity and gradient values of ULF geomagnetic disturbances connected with the Izu strong earthquakes. *Nat. Hazards Earth Syst. Sci.* **2003**, *3*, 211–215. [[CrossRef](#)]
27. Nagao, T.; Enomoto, Y.; Fujinawa, Y.; Hata, M.; Hayakawa, M.; Huang, Q.; Izutsu, J.; Kushida, Y.; Maeda, K.; Oike, K. Electromagnetic anomalies associated with 1995 Kobe earthquake. *J. Geodyn.* **2002**, *33*, 401–411. [[CrossRef](#)]
28. Hattori, K.; Takahashi, I.; Yoshino, C.; Isezaki, N.; Iwasaki, H.; Harada, M.; Kawabata, K.; Kopytenko, E.; Kopytenko, Y.; Maltsev, P.; et al. ULF geomagnetic field measurements in Japan and some recent results associated with Iwateken Nairiku Hokubu earthquake in 1998. *Phys. Chem. Earth* **2004**, *29*, 481–494. [[CrossRef](#)]
29. Serita, A.; Hattori, K.; Yoshino, C.; Hayakawa, M.; Isezaki, N. Principal component analysis and singular spectrum analysis of ULF geomagnetic data associated with earthquakes. *Nat. Hazards Earth Syst. Sci.* **2005**, *5*, 685–689. [[CrossRef](#)]
30. Zhuang, J.; Vere-Jones, D.; Guan, H.; Ogata, Y.; Ma, L. Preliminary analysis of observations on the ultra-low frequency electric field in the Beijing region. *Pure Appl. Geophys.* **2005**, *162*, 1367–1396. [[CrossRef](#)]
31. Telesca, L.; Hattori, K. Non-uniform scaling behavior in ultra-low-frequency (ULF) earthquake-related geomagnetic signals. *Phys. A Stat. Mech. Its Appl.* **2007**, *384*, 522–528. [[CrossRef](#)]
32. Bleier, T.E.; Dunson, C.; Maniscalco, M.; Bryant, N.; Bamberg, R.; Freund, F. Investigation of ULF magnetic pulsations, air conductivity changes, and infra red signatures associated with the 30 October Alum Rock M5.4 earthquake. *Nat. Hazards Earth Syst. Sci.* **2009**, *9*, 585–603. [[CrossRef](#)]
33. Xie, T.; Liu, J.; Lu, J.; Li, M.; Yao, L.; Wang, Y.; Yu, C. Retrospective analysis on electromagnetic anomalies observed by ground fixed station before the 2008 Wenchuan Ms8.0 earthquake. *Chin. J. Geophys. Chin. Ed.* **2018**, *61*, 1922–1937.
34. Chen, C.; Hsu, H.L.; Wen, S.; Yeh, T.; Chang, F.Y.; Wang, C.; Liu, J.; Sun, Y.; Hattori, K.; Yen, H. Evaluation of seismo-electric anomalies using magnetic data in Taiwan. *Nat. Hazards Earth Syst. Sci.* **2013**, *13*, 597–604. [[CrossRef](#)]
35. Huang, Q. Retrospective investigation of geophysical data possibly associated with the Ms8.0 Wenchuan earthquake in Sichuan, China. *J. Asian Earth Sci.* **2011**, *41*, 421–427. [[CrossRef](#)]
36. Huang, Q. Forecasting the epicenter of a future major earthquake. *Proc. Natl. Acad. Sci. USA* **2015**, *112*, 944–945. [[CrossRef](#)]
37. Wen, S.; Chen, C.; Yen, H.; Yeh, T.; Liu, J.; Hattori, K.; Peng, H.; Wang, C.; Shin, T.C. Magnetic storm free ULF analysis in relation with earthquakes in Taiwan. *Nat. Hazards Earth Syst. Sci.* **2012**, *12*, 1747–1754. [[CrossRef](#)]
38. Xu, G.; Han, P.; Huang, Q.; Hattori, K.; Febriani, F.; Yamaguchi, H. Anomalous behaviors of geomagnetic diurnal variations prior to the 2011 off the Pacific coast of Tohoku earthquake (Mw9.0). *J. Asian Earth Sci.* **2013**, *77*, 59–65. [[CrossRef](#)]
39. Ouyang, X.Y.; Parrot, M.; Bortnik, J. ULF Wave Activity Observed in the Nighttime Ionosphere Above and Some Hours Before Strong Earthquakes. *J. Geophys. Res. Space Phys.* **2020**, *125*, e2020JA028396. [[CrossRef](#)]
40. Fraser-Smith, A.C.; Bernardi, A.; McGill, P.R.; Ladd, M.E.; Helliwell, R.A.; Villard, O.G., Jr. Low-frequency magnetic field measurements near the epicenter of the Ms 7.1 Loma Prieta Earthquake. *Geophys. Res. Lett.* **1990**, *17*, 1465–1468. [[CrossRef](#)]
41. Kopytenko, Y.A.; Matiashvili, T.G.; Voronov, P.M.; Kopytenko, E.A.; Molchanov, O.A. Detection of ultra-low-frequency emissions connected with the Spitak earthquake and its aftershock activity, based on geomagnetic pulsations data at Dusheti and Vardzia observatories. *Phys. Earth Planet. Inter.* **1993**, *77*, 85–95. [[CrossRef](#)]
42. Hayakawa, M.; Kawate, R.; Molchanov, O.A.; Yumoto, K. Results of ultra-low-frequency magnetic field measurements during the Guam Earthquake of 8 August 1993. *Geophys. Res. Lett.* **1996**, *23*, 241–244. [[CrossRef](#)]
43. Hattori, K.; Akinaga, Y.; Hayakawa, M.; Yumoto, K.; Nagao, T.; Uyeda, S. ULF magnetic anomaly preceding the 1997 Kagoshima earthquake. *Seism. Electromagn.* **2002**, *353*, 19–28.
44. Uyeda, S.; Hayakawa, M.; Nagao, T.; Molchanov, O.; Hattori, K.; Orihara, Y.; Gotoh, K.; Akinaga, Y.; Tanaka, H. Electric and magnetic phenomena observed before the volcano-seismic activity in 2000 in the Izu Island Region, Japan. *Proc. Natl. Acad. Sci. USA* **2002**, *99*, 7352–7355. [[CrossRef](#)] [[PubMed](#)]

45. Hattori, K.; Serita, A.; Gotoh, K.; Yoshino, C.; Harada, M.; Isezaki, N.; Hayakawa, M. ULF geomagnetic anomaly associated with 2000 Izu Islands earthquake swarm, Japan. *Phys. Chem. Earth* **2004**, *29*, 425–435. [[CrossRef](#)]
46. Hattori, K.; Serita, A.; Yoshino, C.; Hayakawa, M.; Isezaki, N. Singular spectral analysis and principal component analysis for signal discrimination of ULF geomagnetic data associated with 2000 Izu Island Earthquake Swarm. *Phys. Chem. Earth* **2006**, *31*, 281–291. [[CrossRef](#)]
47. Gotoh, K.; Hayakawa, M.; Smirnova, N. Fractal analysis of the ULF geomagnetic data obtained at Izu Peninsula, Japan in relation to the nearby earthquake swarm of June–August 2000. *Nat. Hazards Earth Syst. Sci.* **2003**, *3*, 229–236. [[CrossRef](#)]
48. Telesca, L.; Lapenna, V.; Macchiato, M.; Hattori, K. Investigating non-uniform scaling behavior in Ultra Low Frequency (ULF) earthquake-related geomagnetic signals. *Earth Planet. Sci. Lett.* **2008**, *268*, 219–224. [[CrossRef](#)]
49. Ismaguilov, V.S.; Kopytenko, Y.A.; Hattori, K.; Voronov, P.M.; Molchanov, O.A.; Hayakawa, M. ULF magnetic emissions connected with under sea bottom earthquakes. *Nat. Hazards Earth Syst. Sci.* **2001**, *1*, 23–31. [[CrossRef](#)]
50. Kotsarenko, A.; Molchanov, O.; Hayakawa, M.; Koshevaya, S.; Grimalsky, V.; Enriquez, R.W.; Cruz-Abeyro, J.A.L. Investigation of ULF magnetic anomaly during Izu earthquake swarm and Miyakejima volcano eruption at summer 2000, Japan. *Nat. Hazards Earth Syst. Sci.* **2005**, *5*, 63–69. [[CrossRef](#)]
51. Han, P.; Hattori, K.; Huang, Q.; Hirano, T.; Ishiguro, Y.; Yoshino, C.; Febriani, F. Evaluation of ULF electromagnetic phenomena associated with the 2000 Izu Islands earthquake swarm by wavelet transform analysis. *Nat. Hazards Earth Syst. Sci.* **2011**, *11*, 965–970. [[CrossRef](#)]
52. Hattori, K.; Han, P.; Yoshino, C.; Febriani, F.; Yamaguchi, H.; Chen, C. Investigation of ULF Seismo-Magnetic Phenomena in Kanto, Japan During 2000–2010: Case Studies and Statistical Studies. *Surv. Geophys.* **2013**, *34*, 293–316. [[CrossRef](#)]
53. Schekotov, A.; Molchanov, O.A.; Hayakawa, M.; Fedorov, E.; Chebrov, V.N.; Sinitsin, V.; Gordeev, E.; Belyaev, G.G.; Yagova, N. ULF/ELF magnetic field variations from atmosphere induced by seismicity. *Radio Sci.* **2007**, *42*, 1–13. [[CrossRef](#)]
54. Molchan, G. Structure of optimal strategies in earthquake prediction. *Tectonophysics* **1991**, *193*, 267–276. [[CrossRef](#)]
55. Molchan, G.M.; Kagan, Y.Y. Earthquake prediction and its optimization. *J. Geophys. Res.* **1992**, *97*, 4823–4838. [[CrossRef](#)]
56. Warden, S.; Bleier, T.; Kappler, K. Long term air ion monitoring in search of pre-earthquake signals. *J. Atmos. Sol. Terr. Phys.* **2019**, *186*, 47–60. [[CrossRef](#)]
57. Dunson, J.C.; Bleier, T.E.; Roth, S.; Heraud, J.; Alvarez, C.H.; Lira, A. The Pulse Azimuth effect as seen in induction coil magnetometers located in California and Peru 2007–2010, and its possible association with earthquakes. *Nat. Hazards Earth Syst. Sci.* **2011**, *11*, 2085–2105. [[CrossRef](#)]
58. Kappler, K.N.; Schneider, D.D.; MacLean, L.S.; Bleier, T.E.; Lemon, J.J. An algorithmic framework for investigating the temporal relationship of magnetic field pulses and earthquakes applied to California. *Comput. Geosci.* **2019**, *133*, 104317. [[CrossRef](#)]
59. Heavlin, W.D.; Kappler, K.; Yang, L.; Fan, M.; Hickey, J.; Lemon, J.; MacLean, L.; Bleier, T.; Riley, P.; Schneider, D. Case-control study on a decade of ground-based magnetometers in California reveals modest signal 24–72 h prior to earthquakes. *J. Geophys. Res. Solid Earth* **2022**, *127*, e2022JB024109. [[CrossRef](#)]
60. Yuan, H.H.; Chen, B.; Gu, Z.W.; Ni, Z.; Su, S.P.; Xing, C.J.; Song, C.K. Mobile seismic and geomagnetic monitoring network in China. In Proceedings of the 2018 Annual Meeting of Chinese Geoscience Union, Beijing, China, 21–24 October 2018.
61. Li, Q.; Yuan, Y.; Yang, X.; Cai, S.; Sun, W. Variation of the geomagnetic harmonic wave amplitude ratio before the MS5.5 Eryuan earthquake in 2013. *Acta Seismol. Sin. Chin. Ed.* **2016**, *38*, 122–129.
62. Ma, Q. Multi-dipole observation system and study on the abnormal variation of the geoelectric field observed at Capital network before the 2006 Wen’an, Hebei of China, Ms 5.1 earthquake. *Acta Seismol. Sin. Chin. Ed.* **2008**, *30*, 615–625.
63. Qian, J.; Ma, Q.; Li, S. Further study on the anomalies in apparent resistivity in the NE configuration at Chengdu station associated with Whenchuan Ms 8.0 earthquake. *Acta Seismol. Sin. Chin. Ed.* **2013**, *35*, 4–17.
64. Ma, Q.; Fang, G.; Li, W.; Zhou, J. Electromagnetic anomalies before the 2018 Lushan Ms 7.0 earthquake. *Acta Seismol. Sin. Chin. Ed.* **2021**, *35*, 717–730.
65. Du, X.; Ye, Q.; Ma, Z.; Li, N.; Chen, J.; Tan, D. The detection depth of symmetric four-electrode resistivity observation in/near the epicentral region of strong earthquakes. *Chin. J. Geophys. Chin. Ed.* **2008**, *51*, 1943–1949. [[CrossRef](#)]
66. Tang, J.; Zhao, G.; Jijun, W.; Wenjun, L.; Yan, Z. Variation and analysis of resistivity before and after the Zhangbei-Shangyi earthquake. *Seismol. Geol. Chin. Ed.* **1998**, *20*, 164–171.
67. Chen, J.; Du, X.; Tan, D.; An, Z. Magnetotelluric monitoring of earthquakes in the laohushan fault zone, gansu province. *Earthq. Chin. Ed.* **2009**, *29*, 79–85.
68. Kappler, K.N.; Morrison, H.F.; Egbert, G.D. Long-term monitoring of ULF electromagnetic fields at Parkfield, California. *J. Geophys. Res. Solid Earth* **2010**, *115*, 406. [[CrossRef](#)]
69. Campbell, W.H. Natural magnetic disturbance fields, not precursors, preceding the Loma Prieta earthquake. *J. Geophys. Res. Space Phys.* **2009**, *114*, 307. [[CrossRef](#)]
70. Thomas, J.N.; Love, J.J.; Johnston, M.J.S. On the reported magnetic precursor of the 1989 Loma Prieta earthquake. *Phys. Earth Planet. Inter.* **2009**, *173*, 207–215. [[CrossRef](#)]
71. Masci, F.; Thomas, J.N. Are there new findings in the search for ULF magnetic precursors to earthquakes? *J. Geophys. Res. Space Phys.* **2015**, *120*, 10289–10304. [[CrossRef](#)]
72. Fidani, C. The earthquake lights (EQL) of the 6 April 2009 Aquila earthquake, in Central Italy. *Nat. Hazards Earth Syst. Sci.* **2010**, *10*, 967–978. [[CrossRef](#)]

73. Derr, J. Earthquake lights: A review of observations and present theories. *Bull. Seismol. Soc. Am.* **1973**, *63*, 2177–2187.
74. Tramutoli, V.; Cuomo, V.; Filizzola, C.; Pergola, N.; Pietrapertosa, C. Assessing the potential of thermal infrared satellite surveys for monitoring seismically active areas: The case of Kocaeli (İzmit) earthquake, 17 August 1999. *Remote Sens. Environ.* **2005**, *96*, 409–426. [[CrossRef](#)]
75. Ouzounov, D.; Bryant, N.; Logan, T.; Pulinets, S.; Taylor, P. Satellite thermal IR phenomena associated with some of the major earthquakes in 1999–2003. *Phys. Chem. Earth Parts A/B/C* **2006**, *31*, 154–163. [[CrossRef](#)]
76. Ouzounov, D.; Liu, D.; Chunli, K.; Cervone, G.; Kafatos, M.; Taylor, P. Outgoing long wave radiation variability from IR satellite data prior to major earthquakes. *Tectonophysics* **2007**, *431*, 211–220. [[CrossRef](#)]
77. Jianguo, H. Near earth surface anomalies of the atmospheric electric field and earthquakes. *Acta Seismol. Sin. Engl. Ed.* **1989**, *2*, 289–298.
78. Chen, T.; Li, L.; Zhang, X.-X.; Ma, Q.-M.; Li, W.; Ti, S.; Wu, H.; Li, R.-K.; Luo, J.; Su, J.-F. Near-epicenter weather conditions several hours before strong earthquakes ( $M_s \geq 6$ ). *Nat. Hazards* **2022**, *110*, 57–68. [[CrossRef](#)]
79. Liu, J.Y.; Chen, Y.I.; Huang, C.H.; Ho, Y.Y.; Chen, C.H. A statistical study of lightning activities and  $M \geq 5.0$  earthquakes in Taiwan during 1993–2004. *Surv. Geophys.* **2015**, *36*, 851–859. [[CrossRef](#)]
80. Finkelstein, D.; Hill, R.D.; Powell, J.R. The Piezoelectric Theory of earthquake lightning. *J. Geophys. Res.* **1973**, *78*, 992–993. [[CrossRef](#)]
81. Qin, K.; Wu, L.; De Santis, A.; Wang, H. Surface latent heat flux anomalies before the MS 7.1 New Zealand earthquake 2010. *Chin. Sci. Bull.* **2011**, *56*, 3273. [[CrossRef](#)]
82. Kai, Q. Preliminary analysis of surface temperature anomalies that preceded the two major Emilia 2012 earthquakes (Italy). *Ann. Geophys.* **2012**, *55*, 823–828.
83. Ouzounov, D.; Pulinets, S.; Hattori, K.; Taylor, P. *Pre-Earthquake Processes: A Multidisciplinary Approach to Earthquake Prediction Studies*; John Wiley & Sons: Hoboken, NJ, USA, 2018; Volume 234.
84. Genzano, N.; Filizzola, C.; Hattori, K.; Pergola, N.; Tramutoli, V. Statistical correlation analysis between thermal infrared anomalies observed from MTSATs and large earthquakes occurred in Japan (2005–2015). *J. Geophys. Res. Solid Earth* **2021**, *126*, e2020JB020108. [[CrossRef](#)]
85. Blackett, M.; Wooster, M.J.; Malamud, B.D. Exploring land surface temperature earthquake precursors: A focus on the Gujarat (India) earthquake of 2001. *Geophys. Res. Lett.* **2011**, *38*, 303. [[CrossRef](#)]
86. Zhang, Y.; Meng, Q. A statistical analysis of TIR anomalies extracted by RSTs in relation to an earthquake in the Sichuan area using MODIS LST data. *Nat. Hazards Earth Syst. Sci.* **2019**, *19*, 535–549. [[CrossRef](#)]
87. Galperin, Y.I.; Hayakawa, M. On the magnetospheric effects of experimental ground explosions observed from AUREOL-3. *J. Geomagn. Geoelectr.* **1996**, *48*, 1241–1263. [[CrossRef](#)]
88. Hayakawa, M.; Molchanov, O.A.; Ondoh, T.; Kawai, E. Anomalies in the sub-ionospheric VLF signals for the 1995 Hyogo-ken Nanbu earthquake. *J. Phys. Earth* **1996**, *44*, 413–418. [[CrossRef](#)]
89. Molchanov, O.A.; Hayakawa, M. Subionospheric VLF signal perturbations possibly related to earthquakes. *J. Geophys. Res. Space Phys.* **1998**, *103*, 17489–17504. [[CrossRef](#)]
90. Akhoondzadeh, M.; Parrot, M.; Saradjian, M.R. Investigation of VLF and HF waves showing seismo-ionospheric anomalies induced by the 29 September 2009 Samoa earthquake ( $M_w = 8.1$ ). *Nat. Hazards Earth Syst. Sci.* **2010**, *10*, 1061–1067. [[CrossRef](#)]
91. Shen, X.H.; Zhang, X.M.; Yuan, S.G.; Wang, L.W.; Cao, J.B.; Huang, J.P.; Zhu, X.H.; Piergiorgio, P.; Dai, J.P. The state-of-the-art of the China Seismo-Electromagnetic Satellite mission. *Sci. China Technol. Sci.* **2018**, *61*, 634–642. [[CrossRef](#)]
92. Hayakawa, M.; Molchanov, O.A.; Ondoh, T.; Kawai, E. On the precursory signature of kobe earthquake on VLF subionospheric signals. In Proceedings of the 1997 International Symposium on Electromagnetic Compatibility, Beijing, China, 21–23 May 1997; pp. 72–75.
93. Hayakawa, M.; Ohta, K.; Maekawa, S.; Yamauchi, T.; Ida, Y.; Gotoh, T.; Yonaiguchi, N.; Sasaki, H.; Nakamura, T. Electromagnetic precursors to the 2004 Mid Niigata Prefecture earthquake. *Phys. Chem. Earth Parts A/B/C* **2006**, *31*, 356–364. [[CrossRef](#)]
94. Hayakawa, M. VLF/LF radio sounding of ionospheric perturbations associated with earthquakes. *Sensors* **2007**, *7*, 1141–1158. [[CrossRef](#)]
95. Rozhnoi, A.; Solovieva, M.S.; Molchanov, O.A.; Hayakawa, M. Middle latitude LF (40 kHz) phase variations associated with earthquakes for quiet and disturbed geomagnetic conditions. *Phys. Chem. Earth Parts A/B/C* **2004**, *29*, 589–598. [[CrossRef](#)]
96. Asada, T.; Baba, H.; Kawazoe, M.; Sugiura, M. An attempt to delineate very low frequency electromagnetic signals associated with earthquakes. *Earth Planets Space* **2001**, *53*, 55–62. [[CrossRef](#)]
97. Nagao, T.; Kamogawa, M.; Izutsu, J.; Baba, H.; Narushima, T.; Takamura, N.; Sakurada, T.; Uehara, H. First report of the electromagnetic wave detection system in VLF range, Tokai University—Proven for the existence of preseismic phenomena. *Bull. Inst. Ocean. Research Dev.* **2016**, *37*, 29–36.
98. Moriya, T.; Mogi, T.; Takada, M. Anomalous pre-seismic transmission of VHF-band radio waves resulting from large earthquakes, and its statistical relationship to magnitude of impending earthquakes. *Geophys. J. Int.* **2010**, *180*, 858–870. [[CrossRef](#)]
99. Zhang, X. The development in seismic application research of VLF/LF radio waves. *Acta Seismol. Sin. Chin. Ed.* **2021**, *43*, 656.
100. Zhao, G.Z.; Wang, L.F.; Tang, J.; Chen, X.B.; Zhan, Y.; Xia, Q.B.; Wang, J.J.; Cai, J.T.; Xu, G.J.; Wan, Z.S.; et al. New experiments of CSELF electromagnetic method for earthquake monitoring. *Chin. J. Geophys. Chin. Ed.* **2010**, *53*, 479–486.

101. Parrot, M.; Berthelier, J.J.; Lebreton, J.P.; Sauvaud, J.A.; Santolik, O.; Blecki, J. Examples of unusual ionospheric observations made by the DEMETER satellite over seismic regions. *Phys. Chem. Earth Parts A/B/C* **2006**, *31*, 486–495. [[CrossRef](#)]
102. Zeng, Z.C.; Zhang, B.; Fang, G.Y.; Wang, D.F.; Yin, H.J. The analysis of ionospheric variations before Wenchuan earthquake with DEMETER data. *Chin. J. Geophys. Chin. Ed.* **2009**, *52*, 11–19. [[CrossRef](#)]
103. Akhoondzadeh, M.; Parrot, M.; Saradjian, M.R. Electron and ion density variations before strong earthquakes ( $M > 6.0$ ) using DEMETER and GPS data. *Nat. Hazards Earth Syst. Sci.* **2010**, *10*, 7–18. [[CrossRef](#)]
104. He, Y.; Yang, D.; Qian, J.; Parrot, M. Response of the ionospheric electron density to different types of seismic events. *Nat. Hazards Earth Syst. Sci. Discuss.* **2011**, *11*, 2173–2180.
105. Sarkar, S.; Tiwari, S.; Gwal, A.K. Electron density anomalies associated with  $M \geq 5.9$  earthquakes in Indonesia during 2005 observed by DEMETER. *J. Atmos. Sol. -Terr. Phys.* **2011**, *73*, 2289–2299. [[CrossRef](#)]
106. Parrot, M. Statistical analysis of automatically detected ion density variations recorded by DEMETER and their relation to seismic activity. *Ann. Geophys.* **2012**, *55*, 149–155.
107. Li, M.; Parrot, M. Statistical analysis of an ionospheric parameter as a base for earthquake prediction. *J. Geophys. Res. Space Phys.* **2013**, *118*, 3731–3739. [[CrossRef](#)]
108. Pisa, D.; Nėmec, F.; Santolík, O.; Parrot, M.; Rycroft, M. Additional attenuation of natural VLF electromagnetic waves observed by the DEMETER spacecraft resulting from preseismic activity. *J. Geophys. Res. Space Phys.* **2013**, *118*, 5286–5295. [[CrossRef](#)]
109. Rozhnoi, A.; Solovieva, M.; Parrot, M.; Hayakawa, M.; Biagi, P.-F. VLF/LF signal studies of the ionospheric response to strong seismic activity in the Far Eastern region combining the DEMETER and ground-based observations. *Phys. Chem. Earth Parts A/B/C* **2015**, *85–86*, 141–149. [[CrossRef](#)]
110. Nėmec, F.; Santolík, O.; Parrot, M.; Berthelier, J.J. Spacecraft observations of electromagnetic perturbations connected with seismic activity. *Geophys. Res. Lett.* **2008**, *35*, 109. [[CrossRef](#)]
111. Marchetti, D.; Akhoondzadeh, M. Analysis of Swarm satellites data showing seismo-ionospheric anomalies around the time of the strong Mexico ( $M-w = 8.2$ ) earthquake of 8 September 2017. *Adv. Space Res.* **2018**, *62*, 614–623. [[CrossRef](#)]
112. Marchetti, D.; De Santis, A.; Campuzano, S.A.; Zhu, K.; Soldani, M.; D’Arcangelo, S.; Orlando, M.; Wang, T.; Cianchini, G.; Di Mauro, D.; et al. Worldwide statistical correlation of eight years of swarm satellite data with  $M5.5+$  earthquakes: New hints about the preseismic phenomena from space. *Remote Sens.* **2022**, *14*, 2649. [[CrossRef](#)]
113. Marchetti, D.; De Santis, A.; D’Arcangelo, S.; Poggio, F.; Piscini, A.; Campuzano, S.A.; De Carvalho, W.V.J.O. Pre-earthquake chain processes detected from ground to satellite altitude in preparation of the 2016–2017 seismic sequence in Central Italy. *Remote Sens. Environ.* **2019**, *229*, 93–99. [[CrossRef](#)]
114. De Santis, A.; Marchetti, D.; Pavón-Carrasco, F.J.; Cianchini, G.; Perrone, L.; Abbattista, C.; Alfonsi, L.; Amoroso, L.; Campuzano, S.A.; Carbone, M.; et al. Precursory worldwide signatures of earthquake occurrences on Swarm satellite data. *Sci. Rep.* **2019**, *9*, 20287. [[CrossRef](#)] [[PubMed](#)]
115. Li, M.; Parrot, M. Statistical analysis of the ionospheric ion density recorded by DEMETER in the epicenter areas of earthquakes as well as in their magnetically conjugate point areas. *Adv. Space Res.* **2018**, *61*, 974–984. [[CrossRef](#)]
116. Cao, J.B.; Zeng, L.; Zhan, F.; Wang, Z.G.; Wang, Y.; Chen, Y.; Meng, Q.C.; Ji, Z.Q.; Wang, P.F.; Liu, Z.W.; et al. The electromagnetic wave experiment for CSES mission: Search coil magnetometer. *Sci. China Technol. Sci.* **2018**, *61*, 653–658. [[CrossRef](#)]
117. Li, M.; Shen, X.H.; Parrot, M.; Zhang, X.M.; Zhang, Y.; Yu, C.; Yan, R.; Liu, D.P.; Lu, H.X.; Guo, F.; et al. Primary joint statistical seismic influence on ionospheric parameters recorded by the CSES and DEMETER satellites. *J. Geophys. Res. Space Phys.* **2020**, *125*, e2020JA028116. [[CrossRef](#)]
118. Liu, J.; Guan, Y.B.; Zhang, X.M.; Shen, X.H. The data comparison of electron density between CSES and DEMETER satellite, swarm constellation and IRI model. *Earth Space Sci.* **2021**, *8*, e2020EA001475. [[CrossRef](#)]
119. Yang, Y.Y.; Hulot, G.; Vigneron, P.; Shen, X.H.; Zhima, Z.; Zhou, B.; Magnes, W.; Olsen, N.; Toffner-Clausen, L.; Huang, J.P.; et al. The CSES global geomagnetic field model (CGGM): An IGRF-type global geomagnetic field model based on data from the China seismo-electromagnetic satellite. *Earth Planets Space* **2021**, *73*, 45. [[CrossRef](#)]
120. Yan, R.; Zhima, Z.R.; Xiong, C.; Shen, X.H.; Huang, J.P.; Guan, Y.B.; Zhu, X.H.; Liu, C. Comparison of electron density and temperature from the CSES satellite with other space-borne and ground-based observations. *J. Geophys. Res. Space Phys.* **2020**, *125*, e2019JA027747. [[CrossRef](#)]
121. Shen, X.H.; Huang, J.P.; Lin, J.; Luo, Z.C.; Yue, H.J.; Wu, L.X.; Zhang, X.M.; Cui, J. Project plan and research on data analysis and processing technology of geophysical exploration satellite and application research of earthquake prediction. *Prog. Earthq. Sci. Chin. Ed.* **2022**, *52*, 1–25.
122. Zhima, Z.; Zhou, B.; Zhao, S.; Wang, Q.; Huang, J.; Zeng, L.; Lei, J.; Chen, Y.; Li, C.; Yang, D.; et al. Cross-calibration on the electromagnetic field detection payloads of the China seismo-electromagnetic satellite. *Sci. China Technol. Sci.* **2022**, *65*, 1415–1426. [[CrossRef](#)]
123. Rui, Y.; XuHui, S.; JianPing, H.; Qiao, W.; Wei, C.; DaPeng, L.; YanYan, Y.; HengXin, L.; Song, X. Examples of unusual ionospheric observations by the CSES prior to earthquakes. *Earth Planet. Phys.* **2018**, *2*, 515–526.
124. Song, R.; Hattori, K.; Zhang, X.M.; Sanaka, S. Seismic-ionospheric effects prior to four earthquakes in Indonesia detected by the China seismo-electromagnetic satellite. *J. Atmos. Sol. Terr. Phys.* **2020**, *205*, 105291. [[CrossRef](#)]
125. Zhu, K.; Zheng, L.; Yan, R.; Shen, X.; Zeren, Z.; Xu, S.; Chu, W.; Liu, D.; Zhou, N.; Guo, F. The variations of electron density and temperature related to seismic activities observed by CSES. *Nat. Hazards Res.* **2021**, *1*, 88–94. [[CrossRef](#)]

126. Xiong, P.; Long, C.; Zhou, H.Y.; Battiston, R.; Zhang, X.M.; Shen, X.H. Identification of Electromagnetic Pre-Earthquake Perturbations from the DEMETER Data by Machine Learning. *Remote Sens.* **2020**, *12*, 3643. [[CrossRef](#)]
127. Xiong, P.; Long, C.; Zhou, H.; Battiston, R.; De Santis, A.; Ouzounov, D.; Zhang, X.; Shen, X. Pre-earthquake ionospheric perturbation identification using CSES data via transfer learning. *Front. Environ. Sci.* **2021**, *9*, 514. [[CrossRef](#)]
128. Li, Z.; Yang, B.; Huang, J.; Yin, H.; Yang, X.; Liu, H.; Zhang, F.; Lu, H. Analysis of pre-earthquake space electric field disturbance observed by CSES. *Atmosphere* **2022**, *13*, 934. [[CrossRef](#)]
129. Pulnits, S.; Boyarchuk, K. *Ionospheric Precursors of Earthquakes*; Springer: Cham, The Netherlands, 2004.
130. Liu, J.Y.; Chen, Y.I.; Jhuang, H.K.; Lin, Y.H. Ionospheric foF2 and TEC anomalous days associated with  $M \geq 5.0$  earthquakes in Taiwan during 1997–1999. *Terr. Atmos. Ocean. Sci.* **2004**, *15*, 371–383. [[CrossRef](#)]
131. Liu, J.Y.; Chen, Y.I.; Chuo, Y.J.; Chen, C.S. A statistical investigation of preearthquake ionospheric anomaly. *J. Geophys. Res. Space Phys.* **2006**, *111*, 304. [[CrossRef](#)]
132. Liu, J.Y.; Chen, Y.I.; Chen, C.H.; Liu, C.Y.; Chen, C.Y.; Nishihashi, M.; Li, J.Z.; Xia, Y.Q.; Oyama, K.I.; Hattori, K.; et al. Seismoionospheric GPS total electron content anomalies observed before the 12 May 2008  $M(w)7.9$  Wenchuan earthquake. *J. Geophys. Res. Space Phys.* **2009**, *114*, 320. [[CrossRef](#)]
133. Liu, J.Y.; Chen, Y.I.; Chen, C.H.; Hattori, K. Temporal and spatial precursors in the ionospheric global positioning system (GPS) total electron content observed before the 26 December 2004  $M9.3$  Sumatra-Andaman Earthquake. *J. Geophys. Res. Space Phys.* **2010**, *115*, 312. [[CrossRef](#)]
134. Liu, J.Y.; Le, H.; Chen, Y.I.; Chen, C.H.; Liu, L.; Wan, W.; Su, Y.Z.; Sun, Y.Y.; Lin, C.H.; Chen, M.Q. Observations and simulations of seismoionospheric GPS total electron content anomalies before the 12 January 2010  $M7$  Haiti earthquake. *J. Geophys. Res. Space Phys.* **2011**, *116*, 302.
135. Hirooka, S.; Hattori, K.; Nishihashi, M.; Takeda, T. Neural network based tomographic approach to detect earthquake-related ionospheric anomalies. *Nat. Hazards Earth Syst. Sci.* **2011**, *11*, 2341–2353. [[CrossRef](#)]
136. Hirooka, S.; Hattori, K.; Nishihashi, M.; Kon, S.; Takeda, T. Development of ionospheric tomography using neural network and its application to the 2007 Southern Sumatra earthquake. *Electr. Eng. Jpn.* **2012**, *181*, 9–18. [[CrossRef](#)]
137. Astafyeva, E.; Shalimov, S.; Olshanskaya, E.; Lognonne, P. Ionospheric response to earthquakes of different magnitudes: Larger quakes perturb the ionosphere stronger and longer. *Geophys. Res. Lett.* **2013**, *40*, 1675–1681. [[CrossRef](#)]
138. Guo, J.; Li, W.; Yu, H.; Liu, Z.; Kong, Q. Impending ionospheric anomaly preceding the Iquique  $Mw8.2$  earthquake in Chile on 1 April 2014. *Geophys. J. Int.* **2015**, *203*, 1461–1470. [[CrossRef](#)]
139. Akyol, A.A.; Arıkan, O.; Arıkan, F. A machine learning-based detection of earthquake precursors using ionospheric data. *Radio Sci.* **2020**, *55*, 1–21. [[CrossRef](#)]
140. Heki, K. Ionospheric electron enhancement preceding the 2011 Tohoku-Oki earthquake. *Geophys. Res. Lett.* **2011**, *38*, 312. [[CrossRef](#)]
141. Mukhtarov, P.; Pancheva, D.; Andonov, B.; Pashova, L. Global TEC maps based on GNSS data: 1. Empirical background TEC model. *J. Geophys. Res. Space Phys.* **2013**, *118*, 4594–4608. [[CrossRef](#)]
142. Lim, B.J.M.; Leong, E.C. Challenges in the detection of ionospheric pre-earthquake total electron content anomalies (PETA) for earthquake forewarning. *Pure Appl. Geophys.* **2019**, *176*, 2425–2449. [[CrossRef](#)]
143. Liu, J.Y.; Chen, C.H.; Chen, Y.I.; Yang, W.H.; Oyama, K.I.; Kuo, K.W. A statistical study of ionospheric earthquake precursors monitored by using equatorial ionization anomaly of GPS TEC in Taiwan during 2001–2007. *J. Asian Earth Sci.* **2010**, *39*, 76–80. [[CrossRef](#)]
144. Astafyeva, E.; Heki, K. Vertical TEC over seismically active region during low solar activity. *J. Atmos. Sol. Terr. Phys.* **2011**, *73*, 1643–1652. [[CrossRef](#)]
145. Akhoondzadeh, M. Application of Artificial Bee Colony algorithm in TEC seismo-ionospheric anomalies detection. *Adv. Space Res.* **2015**, *56*, 1200–1211. [[CrossRef](#)]
146. Sompotan, A.; Puspito, N.; Joelianto, E.; Hattori, K. Analysis of ionospheric precursor of earthquake using GIM-TEC, kriging and neural network. *Asian J. Earth Sci.* **2015**, *8*, 32–44. [[CrossRef](#)]
147. Kamogawa, M.; Kakinami, Y. Is an ionospheric electron enhancement preceding the 2011 Tohoku-Oki earthquake a precursor? *J. Geophys. Res. Space Phys.* **2013**, *118*, 1751–1754. [[CrossRef](#)]
148. Masci, F.; Thomas, J.N.; Villani, F.; Secan, J.A.; Rivera, N. On the onset of ionospheric precursors 40 min before strong earthquakes. *J. Geophys. Res. Space Phys.* **2015**, *120*, 1383–1393. [[CrossRef](#)]
149. Iwata, T.; Umeno, K. Correlation analysis for preseismic total electron content anomalies around the 2011 Tohoku-Oki earthquake. *J. Geophys. Res. Space Phys.* **2016**, *121*, 8969–8984. [[CrossRef](#)]
150. Iwata, T.; Umeno, K. Preseismic ionospheric anomalies detected before the 2016 Kumamoto earthquake. *J. Geophys. Res. Space Phys.* **2017**, *122*, 3602–3616. [[CrossRef](#)]
151. Chen, H.; Miao, M.; Chang, Y.; Wang, Q.; Shen, X.; Hattori, K.; Han, P. Singular spectrum analysis of the total electron content changes prior to  $M \geq 6.0$  earthquakes in the Chinese mainland during 1998–2013. *Front. Earth Sci.* **2021**, *9*, 1–12. [[CrossRef](#)]
152. Jhuang, H.-K.; Ho, Y.-Y.; Kakinami, Y.; Liu, J.; Oyama, K.-I.; Parrot, M.; Hattori, K.; Nishihashi, M.; Zhang, D. Seismo-ionospheric anomalies of the GPS-TEC appear before the 12 May 2008  $M7.9$  Wenchuan Earthquake. *Int. J. Remote Sens.* **2010**, *31*, 3579. [[CrossRef](#)]

153. He, L.M.; Wu, L.X.; Pulinets, S.; Liu, S.J.; Yang, F. A nonlinear background removal method for seismo-ionospheric anomaly analysis under a complex solar activity scenario: A case study of the M9.0 Tohoku earthquake. *Adv. Space Res.* **2012**, *50*, 211–220. [[CrossRef](#)]
154. Guo, J.; Shi, K.; Liu, X.; Sun, Y.; Li, W.; Kong, Q. Singular spectrum analysis of ionospheric anomalies preceding great earthquakes: Case studies of Kaikoura and Fukushima earthquakes. *J. Geodyn.* **2019**, *124*, 1–13. [[CrossRef](#)]
155. He, L.M.; Heki, K. Three-dimensional distribution of ionospheric anomalies prior to three large earthquakes in Chile. *Geophys. Res. Lett.* **2016**, *43*, 7287–7293. [[CrossRef](#)]
156. Song, R.; Hattori, K.; Zhang, X.; Liu, J.-Y.; Yoshino, C. Detecting the ionospheric disturbances in Japan using the three-dimensional computerized tomography. *J. Geophys. Res. Space Phys.* **2021**, *126*, e2020JA028561. [[CrossRef](#)]
157. Zhao, G.Z.; Zhang, X.M.; Cai, J.T.; Zhan, Y.; Ma, Q.Z.; Tang, J.; Du, X.B.; Han, B.; Wang, L.F.; Chen, X.B.; et al. A review of seismo-electromagnetic research in China. *Sci. China Earth Sci.* **2022**, *52*, 1229–1246. [[CrossRef](#)]
158. Liu, J.Y.; Chen, Y.I.; Pulinets, S.A.; Tsai, Y.B.; Chuo, Y.J. Seismo-ionospheric signatures prior to  $M \geq 6.0$  Taiwan earthquakes. *Geophys. Res. Lett.* **2000**, *27*, 3113–3116. [[CrossRef](#)]
159. Kon, S.; Nishihashi, M.; Hattori, K. Ionospheric anomalies possibly associated with  $M \geq 6.0$  earthquakes in the Japan area during 1998–2010: Case studies and statistical study. *J. Asian Earth Sci.* **2011**, *41*, 410–420. [[CrossRef](#)]
160. Chen, Y.-I.; Huang, C.-S.; Liu, J.-Y. Statistical evidences of seismo-ionospheric precursors applying receiver operating characteristic (ROC) curve on the GPS total electron content in China. *J. Asian Earth Sci.* **2015**, *114*, 393–402. [[CrossRef](#)]
161. Zhu, F.; Jiang, Y. Investigation of GIM-TEC disturbances before  $M \geq 6.0$  inland earthquakes during 2003–2017. *Sci. Rep.* **2020**, *10*, 18038. [[CrossRef](#)]
162. He, L.M.; Heki, K. Ionospheric anomalies immediately before  $M(w)7.0$ – $8.0$  earthquakes. *J. Geophys. Res. Space Phys.* **2017**, *122*, 8659–8678. [[CrossRef](#)]
163. Chakraborty, S.; Sasmal, S.; Basak, T.; Chakrabarti, S.K. Comparative study of charged particle precipitation from Van Allen radiation belts as observed by NOAA satellites during a land earthquake and an ocean earthquake. *Adv. Space Res.* **2019**, *64*, 719–732. [[CrossRef](#)]
164. Marchitelli, V.; Harabaglia, P.; Troise, C.; De Natale, G. On the correlation between solar activity and large earthquakes worldwide. *Sci. Rep.* **2020**, *10*, 1–10.
165. Dobrovolsky, I.P.; Zubkov, S.I.; Miachkin, V.I. Estimation of the size of earthquake preparation zones. *Pure Appl. Geophys.* **1979**, *117*, 1025–1044. [[CrossRef](#)]
166. Bowman, D.D.; Ouillon, G.; Sammis, C.G.; Sornette, A.; Sornette, D. An observational test of the critical earthquake concept. *J. Geophys. Res. Solid Earth* **1998**, *103*, 24359–24372. [[CrossRef](#)]
167. Jiang, W.; Ma, Y.; Zhou, X.; Li, Z.; An, X.; Wang, K. Analysis of ionospheric vertical total electron content before the 1 April 2014 Mw 8.2 Chile earthquake. *J. Seismol.* **2017**, *21*, 1599–1612. [[CrossRef](#)]
168. Liu, J.Y.; Chen, Y.I.; Chuo, Y.J.; Tsai, H.F. Variations of ionospheric total electron content during the Chi-Chi Earthquake. *Geophys. Res. Lett.* **2001**, *28*, 1383–1386. [[CrossRef](#)]
169. Liu, W.J.; Xu, L. Statistical analysis of ionospheric TEC anomalies before global  $M(w) \geq 7.0$  earthquakes using data of CODE GIM. *J. Seismol.* **2017**, *21*, 759–775. [[CrossRef](#)]
170. Karia, S.P.; Pathak, K.N. Change in refractivity of the atmosphere and large variation in TEC associated with some earthquakes, observed from GPS receiver. *Adv. Space Res.* **2011**, *47*, 867–876. [[CrossRef](#)]
171. Fitterman, D. Calculations of self-potential anomalies near vertical contacts. *Geophysics* **1979**, *44*, 195–205. [[CrossRef](#)]
172. Yoshida, S. Convection current generated prior to rupture in saturated rocks. *J. Geophys. Res.* **2001**, *106*, 2103–2120. [[CrossRef](#)]
173. Yoshida, S.; Ogawa, T. Electromagnetic emissions from dry and wet granite associated with acoustic emissions. *J. Geophys. Res. Solid Earth* **2004**, *109*, 204. [[CrossRef](#)]
174. Freund, F.; Héraud, J.; Centa, V.; Scoville, J. Mechanism of unipolar electromagnetic pulses emitted from the hypocenters of impending earthquakes. *Eur. Phys. J. Spec. Top* **2021**, *230*, 47–65. [[CrossRef](#)]
175. Huang, Q.; Lin, Y. Selectivity of seismic electric signal (SES) of the 2000 Izu earthquake swarm: A 3D FEM numerical simulation model. *Proc. Jpn. Acad. Ser. B* **2010**, *86*, 257–264. [[CrossRef](#)]
176. Enomoto, Y. Coupled interaction of earthquake nucleation with deep Earth gases: A possible mechanism for seismo-electromagnetic phenomena. *Geophys. J. Int.* **2012**, *191*, 1210–1214. [[CrossRef](#)]
177. Shinbrot, T.; Kim, N.H.; Thyagu, N.N. Electrostatic precursors to granular slip events. *Proc. Natl. Acad. Sci. USA* **2012**, *109*, 10806–10810. [[CrossRef](#)]
178. Ren, H.; Chen, X.; Huang, Q. Numerical simulation of coseismic electromagnetic fields associated with seismic waves due to finite faulting in porous media. *Geophys. J. Int.* **2012**, *188*, 925–944. [[CrossRef](#)]
179. Ren, H.; Wen, J.; Huang, Q.; Chen, X. Electrokinetic effect combined with surface-charge assumption: A possible generation mechanism of coseismic EM signals. *Geophys. J. Int.* **2015**, *200*, 837–850. [[CrossRef](#)]
180. Ren, H.; Huang, Q.; Chen, X. Numerical simulation of seismo-electromagnetic fields associated with a fault in a porous medium. *Geophys. J. Int.* **2016**, *206*, 205–220. [[CrossRef](#)]
181. Leeman, J.; Scuderi, M.M.; Marone, C.; Saffer, D.M.; Shinbrot, T. On the origin and evolution of electrical signals during frictional stick slip in sheared granular material. *J. Geophys. Res.* **2014**, *119*, 4253–4268. [[CrossRef](#)]

182. Mizutani, H.; Ishido, T.; Yokokura, T.; Ohnishi, S. Electrokinetic phenomena associated with earthquakes. *Geophys. Res. Lett.* **1976**, *3*, 365–368. [[CrossRef](#)]
183. Fenoglio, M.A.; Johnston, M.J.S.; Byerlee, J.D. Magnetic and electric fields associated with changes in high pore pressure in fault zones: Application to the Loma Prieta ULF emissions. *J. Geophys. Res. Solid Earth* **1995**, *100*, 12951–12958. [[CrossRef](#)]
184. Huang, Q. One possible generation mechanism of co-seismic electric signals. *Proc. Jpn. Acad. Ser. B* **2002**, *78*, 173–178. [[CrossRef](#)]
185. Sasai, Y. Piezomagnetic fields produced by dislocation sources. *Surv. Geophys.* **1994**, *15*, 363–382. [[CrossRef](#)]
186. Gershenzon, N.I.; Gokhberg, M.B.; Yunga, S.L. On the electromagnetic field of an earthquake focus. *Phys. Earth Planet. Inter.* **1993**, *77*, 13–19. [[CrossRef](#)]
187. Draganov, A.B.; Inan, U.S.; Taranenko, Y.N. ULF magnetic signatures at the Earth surface due to ground water flow: A possible precursor to earthquakes. *Geophys. Res. Lett.* **1991**, *18*, 1127–1130. [[CrossRef](#)]
188. Surkov, V. ULF electromagnetic perturbations resulting from the fracture and dilatancy in the earthquake preparation zone. *Atmos. Ionos. Electromagn. Phenom. Assoc. Earthq.* **1999**, *1*, 371–382.
189. Molchanov, O.A.; Hayakawa, M. Generation of ULF electromagnetic emissions by microfracturing. *Geophys. Res. Lett.* **1995**, *22*, 3091–3094. [[CrossRef](#)]
190. Freund, F. Time-resolved study of charge generation and propagation in igneous rocks. *J. Geophys. Res. Solid Earth* **2000**, *105*, 11001–11019. [[CrossRef](#)]
191. Freund, F. Charge generation and propagation in igneous rocks. *J. Geodyn.* **2002**, *33*, 543–570. [[CrossRef](#)]
192. Freund, F. Pre-earthquake signals: Underlying physical processes. *J. Asian Earth Sci.* **2011**, *41*, 383–400. [[CrossRef](#)]
193. Freund, F.; Takeuchi, A.; Lau, B.W.S. Electric currents streaming out of stressed igneous rocks—A step towards understanding pre-earthquake low frequency EM emissions. *Phys. Chem. Earth* **2006**, *31*, 389–396. [[CrossRef](#)]
194. Ren, H.; Huang, Q.; Chen, X. A new numerical technique for simulating the coupled seismic and electromagnetic waves in layered porous media. *Earthq. Sci.* **2010**, *23*, 167–176. [[CrossRef](#)]
195. Gao, Y.X.; Harris, J.M.; Wen, J.; Huang, Y.H.; Twardzik, C.; Chen, X.F.; Hu, H.S. Modeling of the coseismic electromagnetic fields observed during the 2004 M-w 6.0 Parkfield earthquake. *Geophys. Res. Lett.* **2016**, *43*, 620–627. [[CrossRef](#)]
196. Koike, K.; Yoshinaga, T.; Suetsugu, K.; Kashiwaya, K.; Asaue, H. Controls on radon emission from granite as evidenced by compression testing to failure. *Geophys. J. Int.* **2015**, *203*, 428–436. [[CrossRef](#)]
197. Pulnits, S.; Ouzounov, D. Lithosphere-Atmosphere-Ionosphere Coupling (LAIC) model—An unified concept for earthquake precursors validation. *J. Asian Earth Sci.* **2011**, *41*, 371–382. [[CrossRef](#)]
198. Harrison, R.G.; Aplin, K.L.; Rycroft, M.J. Atmospheric electricity coupling between earthquake regions and the ionosphere. *J. Atmos. Sol. Terr. Phys.* **2010**, *72*, 376–381. [[CrossRef](#)]
199. Harrison, R.; Aplin, K.; Rycroft, M. Brief Communication: Earthquake-cloud coupling through the global atmospheric electric circuit. *Nat. Hazards Earth Syst. Sci. Discuss.* **2013**, *1*, 7271–7283. [[CrossRef](#)]
200. Rycroft, M.J.; Nicoll, K.A.; Aplin, K.L.; Giles Harrison, R. Recent advances in global electric circuit coupling between the space environment and the troposphere. *J. Atmos. Sol. Terr. Phys.* **2012**, *90–91*, 198–211. [[CrossRef](#)]
201. Kuo, C.L.; Huba, J.D.; Joyce, G.; Lee, L.C. Ionosphere plasma bubbles and density variations induced by pre-earthquake rock currents and associated surface charges. *J. Geophys. Res. Space Phys.* **2011**, *116*, 317. [[CrossRef](#)]
202. Kuo, C.L.; Lee, L.C.; Huba, J.D. An improved coupling model for the lithosphere-atmosphere-ionosphere system. *J. Geophys. Res. Space Phys.* **2014**, *119*, 3189–3205. [[CrossRef](#)]
203. Shvets, A.V.; Hayakawa, M.; Molchanov, O.A.; Ando, Y. A study of ionospheric response to regional seismic activity by VLF radio sounding. *Phys. Chem. Earth Parts A/B/C* **2004**, *29*, 627–637. [[CrossRef](#)]
204. Liperovsky, V.A.; Meister, C.V.; Liperovskaya, E.V.; Vasil'eva, N.E.; Alimov, O. On spread-E-s effects in the ionosphere before earthquakes. *Nat. Hazards Earth Syst. Sci.* **2005**, *5*, 59–62. [[CrossRef](#)]
205. Sorokin, V.M.; Chmyrev, V.M.; Yaschenko, A.K. Theoretical model of DC electric field formation in the ionosphere stimulated by seismic activity. *J. Atmos. Sol. Terr. Phys.* **2005**, *67*, 1259–1268. [[CrossRef](#)]
206. Zhang, X.M.; Shen, X.H. The development in seismo-ionospheric coupling mechanism. *Prog. Earthq. Sci. Chin. Ed.* **2022**, *52*, 193–202.
207. Liu, J.Y.; Chen, C.H.; Sun, Y.Y.; Chen, C.H.; Tsai, H.F.; Yen, H.Y.; Chum, J.; Lastovicka, J.; Yang, Q.S.; Chen, W.S.; et al. The vertical propagation of disturbances triggered by seismic waves of the 11 March 2011 M9.0 Tohoku earthquake over Taiwan. *Geophys. Res. Lett.* **2016**, *43*, 1759–1765. [[CrossRef](#)]
208. Huang, Q.; Han, P.; Hattori, K.; Ren, H. Electromagnetic Signals Associated With Earthquakes. In *Seismoelectric Exploration*; John Wiley & Sons: Hoboken, NJ, USA, 2020; pp. 415–436.
209. Chen, C.-H.; Sun, Y.-Y.; Lin, K.; Zhou, C.; Xu, R.; Qing, H.; Gao, Y.; Chen, T.; Wang, F.; Yu, H.; et al. A new instrumental array in Sichuan, China, to monitor vibrations and perturbations of the lithosphere, atmosphere, and ionosphere. *Surv. Geophys.* **2021**, *42*, 1425–1442. [[CrossRef](#)]
210. Han, P.; Hattori, K.; Zhuang, J.; Chen, C.; Liu, J.; Yoshida, S. Evaluation of ULF seismo-magnetic phenomena in Kakioka, Japan by using Molchan's error diagram. *Geophys. J. Int.* **2017**, *208*, 482–490. [[CrossRef](#)]
211. Katsumata, K. A long-term seismic quiescence started 23 years before the 2011 off the Pacific coast of Tohoku Earthquake (M = 9.0). *Earth Planets Space* **2011**, *63*, 36. [[CrossRef](#)]

212. Nanjo, K.Z.; Hirata, N.; Obara, K.; Kasahara, K. Decade-scale decrease in  $b$  value prior to the M9-class 2011 Tohoku and 2004 Sumatra quakes. *Geophys. Res. Lett.* **2012**, *39*, 304. [[CrossRef](#)]
213. Sarlis, N.V.; Skordas, E.S.; Varotsos, P.A.; Nagao, T.; Kamogawa, M.; Tanaka, H.; Uyeda, S. Minimum of the order parameter fluctuations of seismicity before major earthquakes in Japan. *Proc. Natl. Acad. Sci. USA* **2013**, *110*, 13734–13738. [[CrossRef](#)]
214. Kato, A.; Obara, K.; Igarashi, T.; Tsuruoka, H.; Nakagawa, S.; Hirata, N. Propagation of slow slip leading up to the 2011 Mw 9.0 Tohoku-Oki earthquake. *Science* **2012**, *335*, 705–708. [[CrossRef](#)]
215. Chen, C.-H.; Wen, S.; Liu, J.-Y.; Hattori, K.; Han, P.; Hobara, Y.; Wang, C.-H.; Yeh, T.-K.; Yen, H.-Y. Surface displacements in Japan before the 11 March 2011 M9.0 Tohoku-Oki earthquake. *J. Asian Earth Sci.* **2014**, *80*, 165–171. [[CrossRef](#)]
216. Ito, Y.; Hino, R.; Kido, M.; Fujimoto, H.; Osada, Y.; Inazu, D.; Ohta, Y.; Iinuma, T.; Ohzono, M.; Miura, S.; et al. Episodic slow slip events in the Japan subduction zone before the 2011 Tohoku-Oki earthquake. *Tectonophysics* **2013**, *600*, 14–26. [[CrossRef](#)]
217. Hattori, K.; Han, P. Investigation on preparation process of the 2011 off the Pacific Coast of Tohoku Earthquake (Mw 9.0) by GPS data. In Proceedings of the 2014 American Geophysics Union Fall Meeting, San Francisco, CA, USA, 15–19 December 2014.
218. Orihara, Y.; Kamogawa, M.; Nagao, T. Preseismic Changes of the level and temperature of confined groundwater related to the 2011 Tohoku earthquake. *Sci. Rep.* **2014**, *4*, 6907. [[CrossRef](#)] [[PubMed](#)]
219. Han, P.; Hattori, K.; Huang, Q.H.; Hirooka, S.; Yoshino, C. Spatiotemporal characteristics of the geomagnetic diurnal variation anomalies prior to the 2011 Tohoku earthquake (Mw 9.0) and the possible coupling of multiple pre-earthquake phenomena. *J. Asian Earth Sci.* **2016**, *129*, 13–21. [[CrossRef](#)]
220. Han, P.; Hattori, K.; Xu, G.J.; Ashida, R.; Chen, C.H.; Febriani, F.; Yamaguchi, H. Further investigations of geomagnetic diurnal variations associated with the 2011 off the Pacific coast of Tohoku earthquake (Mw 9.0). *J. Asian Earth Sci.* **2015**, *114*, 321–326. [[CrossRef](#)]
221. Ogata, Y.; Akaike, H.; Katsura, K. The application of linear intensity models to the investigation of causal relations between a point process and another stochastic process. *Ann. Inst. Stat. Math.* **1982**, *34*, 373–387. [[CrossRef](#)]
222. Zhuang, J.; Matsu'ura, M.; Han, P. Critical zone of the branching crack model for earthquakes: Inherent randomness, earthquake predictability, and precursor modelling. *Eur. Phys. J. Spec. Top.* **2021**, *230*, 409–424. [[CrossRef](#)]